Smart Mater. Struct. **18** (2009) 025008 (9pp) doi:10.1088/0964-1726/18/2/025008

The development of a wireless Love wave biosensor on 41° YX $LiNbO_3$

Hae-Kwan Oh, Wen Wang, Keekeun Lee, Churlki Min and Sangsik Yang

Department of Electronics Engineering, Ajou University, Suwon 443-749, Korea

E-mail: keekeun@ajou.ac.kr

Received 8 April 2008, in final form 28 November 2008
Published 13 January 2009
Online at stacks.iop.org/SMS/18/025008

Abstract

This paper presents a novel wireless Love-wave-based biosensor using a polymethyl methacrylate (PMMA) waveguide and protein A receptor layers on a 41° YX $LiNbO_3$ piezoelectric substrate for immunoglobulin G (IgG) detection. A 440 MHz reflective delay line composed of single-phase unidirectional transducers (SPUDTs) and three shorted grating reflectors was fabricated as the sensor element. A theoretical modeling was performed to describe the wave propagation of Love wave devices on a 41° YX $LiNbO_3$ piezoelectric substrate with large piezoelectricity. The fabricated devices were wirelessly characterized by using the network analyzer as the reader unit. The resultant reflection peaks showed large signal/noise ratio, sharp peaks, and few spurious signals. The binding of the IgG to the protein A receptor layer induced large phase shifts of the reflection peaks due to the mass loading effect. Good linearity, reproducibility, and high sensitivity were observed in the IgG concentration range 1–65 nM. Unique advantages such as high sensitivity and a simple wireless measurement method over other currently available biosensors are also presented.

(Some figures in this article are in colour only in the electronic version)

1. Introduction

In recent years, interest in Love-wave-based devices is increasing in physical, chemical and bio-sensing applications because these Love-wave devices provide low acoustic loss in contact with liquid, high sensitivity, and good protection of the interdigital transducers (IDTs) from harsh gas and liquid environments [1]. These devices also offer low cost, a simple fabrication procedure, portability, and reusability. Typical Love-wave-based biosensors are composed of a piezoelectric substrate supporting a shear horizontal surface acoustic wave (SH SAW), a thin overlayer (waveguide layer) on the top of the substrate, and a receptor layer which responds to a specific biocell. Necessary conditions for obtaining Love wave propagation in the guiding layer are that the substrate should support the SH wave propagation and the shear velocity in the guiding layer should be lower than that in the substrate. Because of the shear nature of the Love wave, Love-wave-based devices can operate in the presence of liquid without any vertical acoustic radiation losses by the mode conversion. There exists an optimal waveguide layer thickness which provides maximum sensitivity to surface mass loading. At this optimal thickness, most of the generated Love wave flows to the upper surface of the waveguide layer, so it provides high sensitivity to surface mass perturbation.

Several kinds of Love wave biosensors with different designs and geometries have been successfully reported. In general, a Love-mode acoustic wave is obtained using a single guiding layer of sputtered silica (SiO_2) [2–8], photoresist, and polymer [9–14], or a multilayer of SiO_2 and polymethyl methacrylate (PMMA) [15, 16]. Polymeric waveguide materials with optimum thickness are more efficient than SiO_2 in converting the bulk SH mode to the Love wave mode due to their lower shear velocity and lower density, resulting in an order of magnitude improvement in mass sensitivity. However, polymeric materials are usually lossy due to their viscoelastic nature [17]. Despite some reported success stories, present Love wave biosensors still suffer from a complicated measurement system using the oscillator as the sensor element structured by a resonator/delay line, and weak sensitivity of the frequency and phase response. Also, an active oscillator structure cannot be used in a wireless biosensor application due to the power system being under some harsh and dangerous environments.

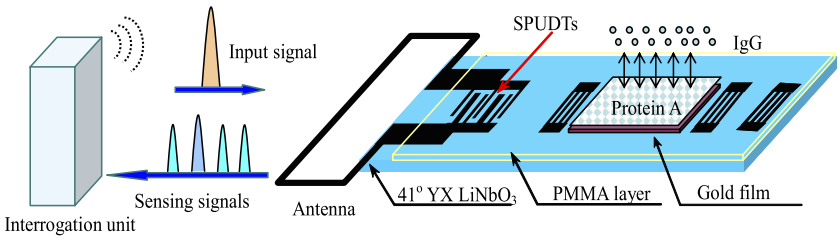

Figure 1. Schematic diagram of the developed Love wave mode biosensor system.

In this paper, we introduce a novel wireless Love-wave-based immunoglobulin G (IgG) biosensor with operating frequency of 440 MHz, which utilizes a 41° YX $LiNbO_3$ substrate with a reflective delay line configuration and a PMMA guiding layer supporting the Love wave propagation. Figure 1 shows a schematic diagram of the developed wireless biosensor system. When the single phase unidirectional transducers (SPUDTs) of the Love wave devices receive electromagnetic (EM) energy from the network analyzer (interrogation unit) through antennas, a Love wave is generated on the interface of PMMA/substrate, propagating toward the reflectors. The propagating Love wave is partially reflected from the reflectors and the reflected wave is reconverted into EM waves by the SPUDTs and transmitted to the measurement system through the antenna. The binding of different concentrations of IgG to the protein A receptor layer induces a change in mass loading and Love wave velocity, resulting in the phase shifts of the reflection peaks. By evaluating the phase shifts, we can extract the IgG concentration. A 41° YX $LiNbO_3$ was used for the piezoelectric substrate because it provides a leaky SH wave mode with high velocity (4792 m s^{-1}) and large electromechanical coupling factor (17.2%), which will be of benefit for the loss mechanism improvement of Love wave devices [18]. PMMA was chosen as the waveguide layer because it has a relatively low density (1.17 g cm^{-3}), low SH velocity (1105 m s^{-1}), and good elastic property [19]. This sensor presents many advantages over currently available other biosensors: (1) it is absolutely passive and does not require a battery or any power supply to operate, (2) it does not need a complicated measurement system owing to the passive sensor element, and (3) it is small, light, and can withstand extremely harsh environmental conditions. To extract the optimal design parameters of the Love wave devices, a theoretical model was proposed and the mass sensitivity was then evaluated. Using the extracted design parameters, the device was fabricated and then wirelessly characterized using a radiofrequency (RF) network analyzer.

2. Design considerations

The primary goals of our Love-wave-based biosensor are high signal/noise (S/N) ratio, sharp reflection peaks, high sensitivity, and long wireless reading distance. The piezoelectric substrate, IDT and reflector geometry, PMMA waveguide layer thickness, sensitive receptor molecule, and measurement method were taken into account to find the optimized device performance.

2.1. SH SAW reflective delay line

41° YX $LiNbO_3$ was used for the piezoelectric substrate because it has a relatively high SH velocity and large electromechanical coupling coefficient, K^2. A larger SH velocity difference between the substrate and the waveguide layer allows greater coupling to a Love wave, so that most of the elastic wave generated from the SPUDTs is converted into the Love wave flowing along the waveguide layer. Higher K^2 allows higher reflectivity from the reflectors and lower insertion loss. The basic idea of the SPUDT is to enhance the generated signal in the forward direction but reduce the signal in the reverse direction using the distributed reflection sources ($\lambda/4$ reflection electrode), which suppress triple transit and reduce the insertion loss effectively [20]. The device was targeted to 440 MHz, so the widths of the SPUDTs were 1.1 and 2.5 μm, respectively. Of several different reflector structures, a shorted grating reflector was chosen because it allows high reflection from the reflector and low insertion loss from the reflector itself [20]. The first reflector was used for the reference reflection peak, and the second and third reflectors were used for temperature compensation. The time interval between the SPUDTs and the first reflector was set to 1.2 μs. This allowed adequate separation between environmental noise echoes and reflection peaks, because all of the environment echoes fade away within $\sim$1 μm.

2.2. Waveguide layer

Of several different waveguide layer materials (e.g., SiO_2, PMMA, photoresist, or a multilayer of SiO_2/PMMA/ZnO), PMMA was chosen for the waveguide layer material, because it has a relatively low density (1.17 g cm^{-3}), low SH velocity (1105 m s^{-1}), good elastic property, and high stiffness modulus (1.7 GPa). Generally, an ideal waveguide material should have the following properties: (1) low shear velocity compared to the substrate, (2) high elastic property, (3) low density, (4) low acoustic absorption, (5) good physical/chemical resistance in aqueous or harsh environments, and (6) uniform surface profile. The sensitivity depends on the properties of the waveguide layer material. The lower the shear wave velocity and the density of the guiding layer, the higher the sensitivity. There exists an optimal waveguide layer thickness which provides maximum sensitivity to surface mass loading. Further increase above the optimum thickness decreases the sensitivity; this is because over-confinement of the wave to the upper surface of the overlayer increases the coupling to the liquid medium, and

the insertion loss (acoustic absorption) in the overlayer itself is also increased. If the waveguide thickness is too thin, the waveguide layer does not efficiently trap the acoustic energy near the sensing surface. From the theoretical simulation works, we found an optimal PMMA waveguide thickness of ∼1.5 μm. A non-smooth surface of the waveguide layer causes extra viscosity, so it can result in an increased insertion loss of the device, causing deterioration in the performance of the device in the liquid media. Also, the thickness of the gold film deposited onto the PMMA guiding layer surface is very thin (∼50 nm), far less than the PMMA thickness. A non-uniform PMMA surface can induce an imperfection of the gold film, resulting in a decrease of the protein A immobilization onto the gold surface, which will influence the IgG bonding directly. Thus, great care during fabrication is necessary to obtain uniform PMMA flatness.

2.3. Immobilization of receptor molecule

Protein A was chosen for the receptor layer because it has high affinity with immunoglobulin G (IgG). To immobilize the protein A onto the gold surface, an absorption method was employed. The sensitivity is strongly related to the high density and stable immobilization of receptor molecules on the gold surface over time. Protein A has a strong affinity for gold, so a very thin gold film (∼50 nm) was deposited onto the PMMA guiding layer because a thick gold film can interfere with the propagation of the Love wave [9, 13]. Protein A was immobilized on the region between the first and second reflectors. The total area of the sensitive film was 3.5 mm × 1 mm to expose a large area to IgG. A 440 MHz central frequency was chosen. Generally it is known that higher operating frequency provides better sensitivity than lower frequency. However, an extremely high central frequency makes the device fabrication more difficult because it requires small dimensions of the IDT and reflectors. So we chose a device with a 440 MHz resonant frequency.

3. Theoretical analysis

3.1. Love wave model

For the theoretical approach, the Love wave device can be considered as a multilayer composed of a semi-infinite piezoelectric substrate and a guiding layer. The piezoelectric substrate acts as a mechanical support and allows generating elastic waves by IDTs. For a Love wave in an isotropic structure, the solution was given by Royer *et al* [21]. In addition, Zimmermann *et al* presented the weak piezoelectric Love wave structure in a substrate like quartz [22]. Kielczynski established the theory of Love waves propagating in a lossy viscoelastic layer deposited on an elastic substrate, in which the attenuation induced by the lossy guiding layer was described numerically [23]. In this paper, we propose a theoretical propagation solution of Love wave in a multilayer structure composed of an anisotropic substrate with large piezoelectricity (using the example of 41° YX $LiNbO_3$ with Eular angles of $(0, -49, 0)$), a guiding layer, and a sensitive layer. The guiding layer and the sensitive layer are considered isotropic. The coordinate system for the Love wave propagation analysis is shown in figure 2. The acoustic wave propagates along the x_1 axis on the x_1–x_2 plane at $x_3 = 0$. The attenuation coefficient of the PMMA guiding layer on Love wave propagation is calculated approximately with reference to the numerical method of [23].

A necessary condition for obtaining Love wave propagation in the guiding layer is shear horizontal polarization. Symmetry properties in the structures considered in this paper allow the reduction of the equations of motion to a single displacement equation and electrical potential for the substrate:

$$\rho_p \partial^2 u_2/\partial t^2 = C_{66}\partial^2 u_2/\partial x_3^2 + C_{44}\partial^2 u_2/\partial x_3^2 + e_{16}\partial^2\phi/\partial x_1^2 + e_{34}\partial^2\phi/\partial x_3^2 \quad (1)$$

$$e_{16}\partial^2 u_2/\partial x_1^2 + e_{34}\partial^2 u_2/\partial x_3^2 = \varepsilon_{11}\partial^2\phi/\partial x_1^2 + \varepsilon_{33}\partial^2\phi/\partial x_3^2.$$

Here u_2 is the acoustic displacement of particles in the x_2 direction, C_{44}, and C_{66} are subscript abbreviations of stiffness constants, e_{16} is the piezoelectric modulus, ε_{33} is the component of permittivity, and ρ_p is the density of the considered layer. The displacement motion equation in the waveguide layer and sensitive film can be described as the following, with shear modulus G_s/G_g and density ρ_s/ρ_g of the guiding layer and the sensitive film:

$$G_{s/g}\partial^2 u_2/\partial x_3 + (\rho_{s/g}\omega^2 - k^2 G_{s/g})u_2 = 0. \quad (2)$$

Based on the mechanical (zero stress at the top of the structure, continuity of stress and mechanical displacement at interfaces between the adjacent layers) and electrical (electric displacement continuity at the interface between the substrate and guiding layer) boundary conditions, the dispersion relation describing the Love wave propagation in the $LiNbO_3$/PMMA/gold can be written as

$$\begin{aligned}
h_g &= \frac{1}{k\alpha_g} \times \arctan((G_g\alpha_g(\lambda_1\lambda_4 + \lambda_2\lambda_3)) \\
&\quad - i\lambda_5(\lambda_1 + \lambda_2))/(iG_g^2\alpha_g^2(\lambda_1 + \lambda_2) + \lambda_1\lambda_4\lambda_5 + \lambda_2\lambda_3\lambda_5) \\
&\quad + n\pi/(k\alpha_g) \\
\alpha_g &= \sqrt{\rho_g v_{Love}/G_g - 1}, \qquad \alpha_s = \sqrt{\rho_s v_{Love}/\mu_s - 1} \\
\lambda_1 &= i\varepsilon_{33}\alpha_{p1}k_1 - ie_{16}\alpha_{p1} - \varepsilon_0 k_1, \\
\lambda_2 &= \varepsilon_0 k_2 + ie_{16}\alpha_{p2} - i\varepsilon_{33}\alpha_{p2}k_2 \\
\lambda_3 &= C_{44}\alpha_{p1} + e_{16}k_1\alpha_{p1}, \qquad \lambda_4 = C_{44}\alpha_{p2} + e_{16}k_2\alpha_{p2} \\
\lambda_5 &= G_s\alpha_s \tan(\alpha_s k h_s), \\
k_1 &= (\rho v_{Love}^2 - C_{66} - C_{44}\alpha_{p1}^2)/(e_{16} + e_{16}\alpha_{p1}^2) \\
k_2 &= (\rho v^2 - C_{66} - C_{44}\alpha_{p2}^2)/(e_{16} + e_{16}\alpha_{p2}^2),
\end{aligned} \quad (3)$$

where n is an integer which represents mode order, α_{p1} and α_{p2} are decay constants for $LiNbO_3$, v_{Love} is the Love wave velocity, and h_g and h_s are the thicknesses of the guiding layer and the sensitive layer.

Owing to the viscoelastic nature of polymer materials, the attenuation induced by the polymer guiding layer on wave propagation should be taken into account. In this paper, we assume that the dispersion relationship of the Love wave propagation is complex with the complex wavevector k (k =

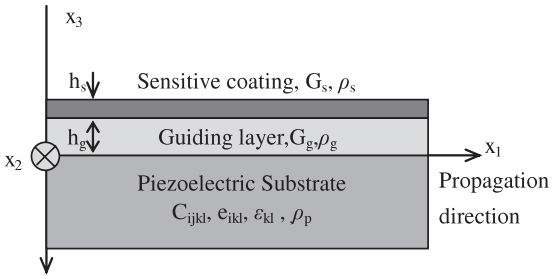

Figure 2. The coordinate system for the Love wave propagation analysis.

$k_0 + j\alpha$, the real part of the wavevector k_0 describes the phase velocity of the Love wave and the imaginary part of the wavevector α is an attenuation coefficient of the Love wave induced by the polymer guiding layer) and complex shear modulus of the guiding layer G_g ($G = G' + jG''$, G' is the storage shear modulus of the PMMA and G'' represents the loss modulus). To simplify the numerical calculation, we neglect the piezoelectric properties of the $LiNbO_3$ substrate. Through the Taylor series expansion mentioned in [23], the attenuation coefficient of the PMMA with thickness h on the wave propagation can be obtained as follows:

$$\alpha h = -\frac{G''}{G'} \times \frac{\frac{1}{2\cos^2(Ah)}\frac{\rho g v^2}{G'}(k_0 h)^2 + \tan(Ah)[\frac{1}{2Ah}\frac{\rho g v^2 (k_0 h)^2}{G'} - Ah]}{\frac{k_0 h}{\cos^2(Ah)} + \frac{\rho_s C_{44} k_0 h}{BG'h(C_{44}C_{66}-C_{46})} + \tan(Ah)\frac{k_0 h}{Ah}}$$
$$A = \sqrt{\rho_g w^2/G' - k_0^2},$$
$$B = \sqrt{k_0^2 - w^2\rho_s C_{44}/(C_{44}C_{66} - C_{46})}. \quad (4)$$

3.2. Mass loading sensitivity

The mass loading effect is modeled by considering that sorption of biochemical compounds modifies only the sensitive layer density (ρ_s). The mass loading effect is taken into account by taking a sensitive layer density increase of $\Delta\rho_s$. In our device structure, the mass loading sensitivity, which is defined by the phase shift $\Delta\Phi$ (or the time shift $\Delta\tau$) between the first and second reflectors due to IgG binding, can be obtained by the fractional change of the propagation velocity at a given sensitive film thickness:

$$\Delta\Phi = 2\pi f_0 \Delta\tau = 2\pi f_0 \times 2l_1/v_0 \times (\Delta v/v_0). \quad (5)$$

Here f_0 is the central frequency, l_1 is the distance between the first and second reflectors, Δv is the phase velocity shift due to mass loading effect, and v_0 is the Love wave phase velocity without mass effect, which is calculated with a waveguide layer thickness of h_g and sensitive film thickness of h_s in equation (3). However, due to large temperature coefficient of delay (TCD, 80 ppm °C^{-1}) of $LiNbO_3$, the phase shift, $\Delta\Phi$, in equation (5) includes the bio and temperature information. To compensate the temperature effect, the mass loading sensitivity was obtained using the method of difference (MOD) [24],

$$\Delta\Phi = (\Delta\Phi_{2-1}) - w(\Delta\Phi_{3-2}), \quad (6)$$

where $\Delta\Phi_{2-1}$ is the phase shift between the first and second reflectors, $\Delta\Phi_{3-2}$ is the phase shift between the second and third reflectors, and w is the ratio of the first-to-second reflector distance to the second-to-third reflector distance.

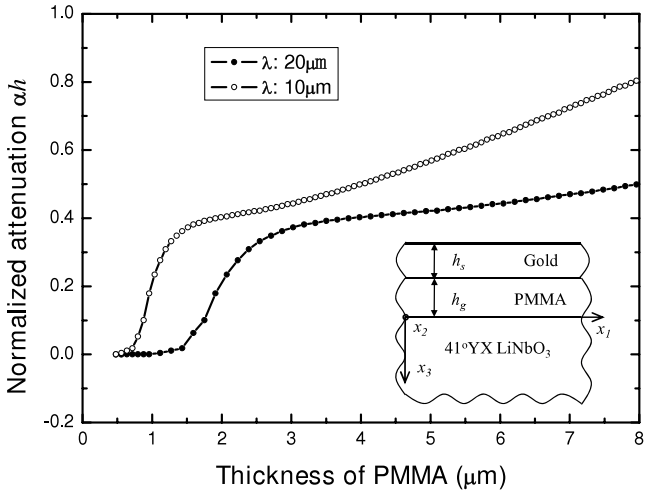

Figure 3. The attenuation coefficient versus PMMA guiding layer thickness as a function of different operation frequency.

3.3. Numerical results and discussion

In this section, we illustrate the numerical results of the fundamental properties of a Love wave in a layered structure of $LiNbO_3$/PMMA/gold. The stiffness constants, piezoelectric moduli, and permittivity constants of $LiNbO_3$ are listed in table 1 [25].

Attenuation coefficient versus PMMA guiding layer thickness. The dispersion curves of the attenuation coefficient αh versus PMMA thickness h at different operation frequencies (represented as different wavelengths, 10λ and 20λ) were calculated from equation (4), as shown in figure 3. The attenuation coefficient αh increases with the guiding layer thickness. The higher the operation frequency, the larger the attenuation coefficient αh. For the Love wave device with low operation frequency (20λ), the attenuation induced by the guiding layer is small in the PMMA thickness range of less than 2 μm, whereas for the device with high operation frequency (10λ), the attenuation increases quickly in the same thickness range. From the calculated results, we found that the PMMA guiding layer with larger thickness induces higher acoustic attenuation. This suggests that the lossy nature of the polymer film determines the optimum guiding layer thickness and should be taken into account when designing an efficient Love wave device.

Table 1. Material parameters of $LiNbO_3$.

Material	Stiffness constants (N m^{-2})	Piezoelectric moduli (C m^{-2})	Permittivity constants ($10^{-10} \times$ F m^{-1})	Density (kg m^{-3})
$LiNbO_3$	C_{11}:20.3; C_{33}:24.5; C_{33}:24.5; C_{44}:6.0; C_{12}:5.3; C_{13}:7.5; C_{14}:0.9	e_{15}:3.7; e_{22}:2.5; e_{31}:0.2; e_{33}:1.3	ε_{11}:3.89576; ε_{33}:2.56766	4700

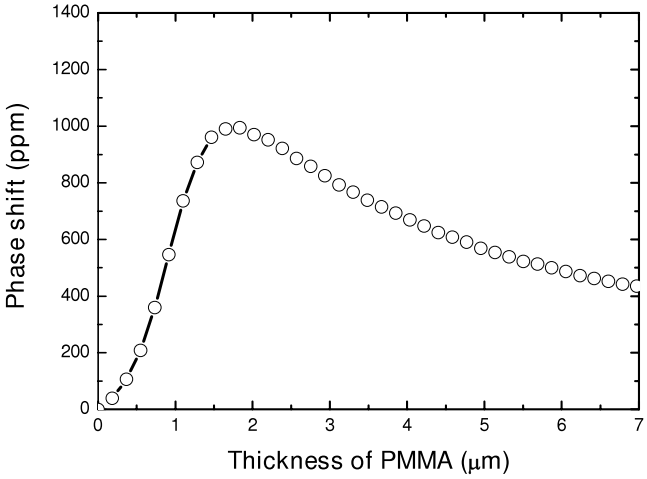

Figure 4. The phase shifts as a function of different PMMA thickness for the Love wave device with fractional thickness kh_s of 0.01.

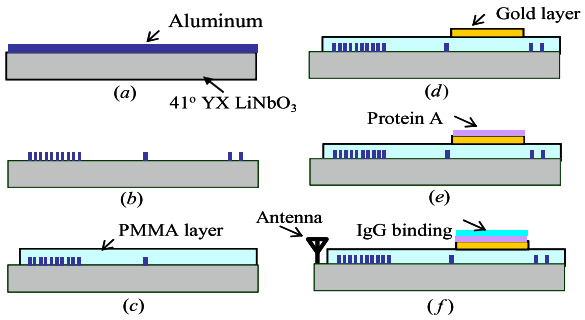

Figure 5. Fabrication procedure of a Love wave sensor. (*a*) Al deposition, (*b*) IDT and reflector pattern, (*c*) PMMA spin coating, (*d*) gold thermal deposition, (*e*) protein A coating, and (*f*) protein–IgG binding.

Guiding layer thickness effect on the mass sensing. When plotting the mass sensitivity (velocity shift) versus guiding layer thickness, the maximum sensitivity is observed at a certain guiding layer thickness. Figure 4 shows the phase shifts as a function of different PMMA thickness for the device composed of 41° YX $LiNbO_3$ substrate, PMMA guiding layer, and gold film with fractional thickness (kh_s) of 0.01 from equation (3). From the simulation results, we consider that the optimum waveguide thickness is approximately 1.5–2 μm.

4. Technique realization

4.1. Fabrication of SH SAW devices on 41° *YX* $LiNbO_3$ *substrate*

Figure 5 shows schematic diagrams of the fabrication procedure. A 4″ 41° YX $LiNbO_3$ with 500 μm thickness was used for the piezoelectric substrate. A ∼150 nm thick layer of aluminum was deposited on the piezoelectric substrate using an electron beam evaporator. Photoresist (PR) was spin-coated, exposed and then patterned for the IDT and reflectors. The aluminum was wet-etched. The PR was dissolved in acetone. Several rinses with deionized (DI) water were performed to remove any unwanted products.

4.2. Waveguide layer

After completing the SH SAW reflective delay line, a layer of polymethylmethacrylate (PMMA) was spin-coated over the entire surface of the $LiNbO_3$ substrate with different spin rates. Different spin rates induce different thicknesses of PMMA. The thickness was targeted from 0.3 to 2 μm. Then the PMMA was cured for 2 h at 180 °C to remove all the solvents.

4.3. Protein A immobilization

To eliminate the acoustic–electric interactions induced by the piezoelectric substrate and dielectric or conducting liquid samples, and to improve the affinity of the protein A, a ∼50 nm thick gold layer was patterned on the PMMA surface between the first and second reflectors using lift-off processing. The device was placed in a sealed container and exposed to PBS buffer (phosphate buffered saline tablets (0.01 M phosphate, 2.7 mM potassium chloride, and 0.137 M sodium chloride, pH 7.4)), which was then shaken at 100 rpm by a shaker for approximately 1 h. Next, protein A was added to the PBS buffer to make a solution of 50 mg ml^{-1} protein A. The concentration of the protein A was high enough to saturate absorption sites on the gold surface. It is well known that the protein A concentration in solution influences the response time of the immobilization onto the gold surface. Larger protein A concentration will reduce the immobilization time. However, there is almost no influence of the protein A concentration on the IgG bonding as long as sufficiently dense protein A immobilization is ensured. Using the experimental data from [13], 50 mg ml^{-1} protein A was used in this paper. The container was shaken again at the same rpm rate for 30 min to immobilize the protein A on the gold surface. Protein A molecules were immobilized on the region between the first and second reflectors. After absorption, the device was thoroughly rinsed in PBS to wash off the weakly attached protein A molecules and then dried.

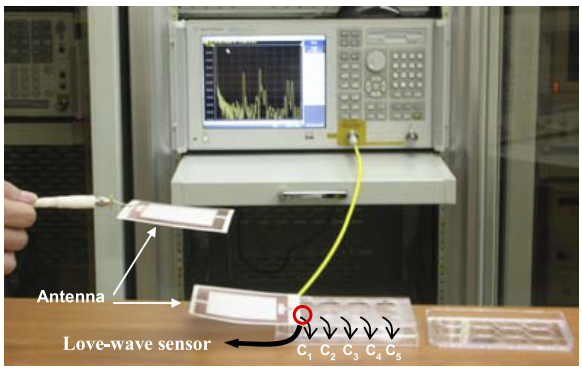

Figure 6. Wireless measurement setup of the biosensor system.

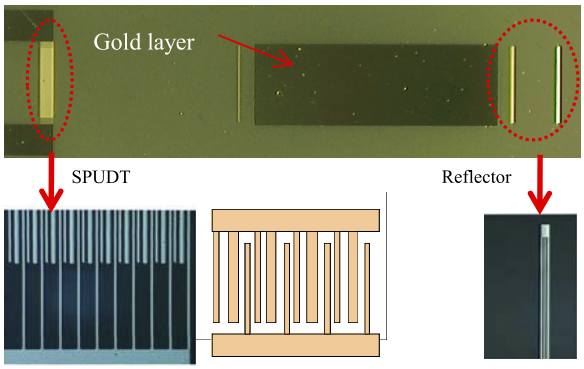

Figure 7. Optical microscope views of the fabricated devices.

4.4. Wireless measurement

For wireless measurement, two two-dimensional planar antennas (10 cm × 10 cm) with 440 MHz operation frequency and 21 MHz bandwidth were fabricated using an 8 mil thick RO4003 substrate (dielectric constant $k = 3.38$). The fabricated antennas were connected to the S_{11} port of the network analyzer and the fabricated Love wave biosensor. The fabricated biosensor was dipped into various IgG solutions in the concentration range 1–65 nM. The reflection coefficient S_{11} was wirelessly measured using the network analyzer, as shown in figure 6. A parabolic approximation method was used to determine the exact position of the reflection peaks [26].

5. Results

5.1. Fabricated devices

Figure 7 shows optical microscope views of the fabricated devices. The number of SPUDT finger pairs was 20, and the finger widths were ∼1.244 mm and 2.488 mm, respectively. The length of the aperture was 100 λ (∼1 mm). Three shorted grating reflectors were arranged in a row on the 41° YX $LiNbO_3$ substrate. The distance between the SPUDT and the first reflector was 2.672 mm, and the distance between the first reflector and the second reflector was 3.95 mm. The ratio of the distance between the first and second reflectors to the distance between the second and third reflectors was 5. PMMA thickness was varied from 0.3 to 2 μm to find an optimized waveguide layer thickness. A uniform waveguide surface was obtained over the delay line regions. The total area of the protein A receptor layer was 3.5 mm × 1 mm.

5.2. Wireless measurement

The fabricated Love wave device with a ∼1.5 μm thick PMMA waveguide layer was wirelessly characterized in air by using the network analyzer as the reader unit. As shown in figure 8, four reflection peaks from three reflectors and gold film were observed in the time domain. The peaks showed large S/N ratio, sharp peaks, and few spurious signals. The first reflection peak occurred at 1.2 μs, and at that point, S_{11} was ∼45 dB. The second reflection peak was observed at 1.8 μs, which results from the gold layer. The RF power from the network analyzer

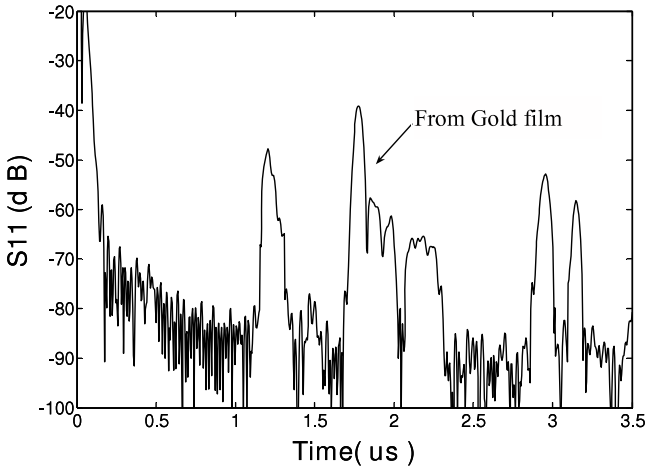

Figure 8. Measured reflection coefficient S_{11} of the Love wave device in the time domain in the case of no IgG binding.

was varied from −40 to 10 dBm (10 mW) to find the maximum readout distance. As the applied RF power increased, the readout distance also increased. With a 10 mW RF power from the network analyzer, a 50 cm readout distance was observed.

5.3. Waveguide thickness effect

Different waveguide thicknesses were spin-coated on the piezoelectric substrate, and the efficiency of each waveguide was compared by monitoring the resonant frequency and insertion loss of the device in air. Figure 9 shows the changes in the resonant frequency f_o and amplitude of the reflection coefficient S_{11} in frequency domain as a function of the overlayer thickness. The PMMA coating on the leaky SH SAW device is expected to affect the velocity of the acoustic wave. This is clearly shown in figure 9, in which the resonant frequency of Love wave device decreases as the thickness of the PMMA increases. The decrease of the resonant frequency is considered to be a decrease of the shear velocity of the Love wave when thicker PMMA polymer layers are applied. The resonant frequency change is zero when the thickness of the waveguide layer is zero.

Figure 9 also shows the changes in the amplitude of the reflection coefficient S_{11} as the PMMA thickness increases,

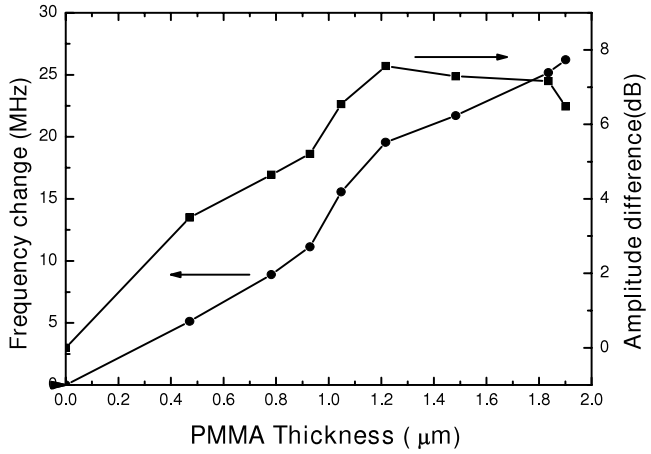

Figure 9. The changes of the resonance frequency and the amplitude of the reflection coefficient S_{11} as a function of PMMA thickness.

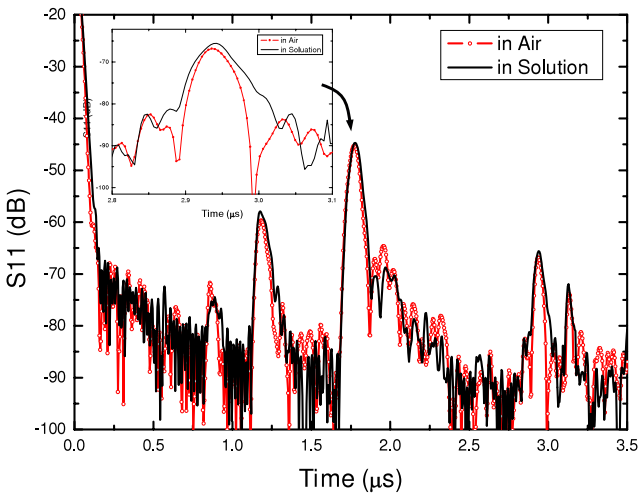

Figure 10. Comparison of the values of S_{11} measured in air and liquid solution.

where the amplitude change is obtained by subtracting the amplitude of the uncoated device from the amplitude of the waveguide-coated device. Positive amplitude changes are observed, indicating that the waveguide devices are less lossy than the leaky SH SAW device, because more acoustic energy is efficiently transduced by the SPUDTs as the wave is guided by the overlayer. Figure 9 shows that amplitude change sharply increases with increasing PMMA thickness up to a thickness of ∼1 μm and then reaches a plateau for thicknesses between 1 and 1.8 μm. For PMMA waveguide layers over 2 μm thick, the amplitude is a little bit decreased, even though it is still considerably larger than that of the uncoated device. The decrease in the amplitude changes can be explained by an increased acoustic loss inside the waveguide layer, which becomes significant when thicker PMMA layers are coated on the device surface. From the measured results, the optimum waveguide thickness is considered as 1.2–1.8 μm, which agrees well with the simulated results. Generally, figures 9 can be used as a guideline for assessing the efficiency of other overlay materials to act as a waveguide layer and support a Love wave.

5.4. Liquid loading effect

Dipping the SAW devices into a liquid solution can cause a vertical radiation loss of the acoustic energy propagating on the top of the liquid samples due to a change in mass density, elastic stiffness, viscosity, and dielectric constant, which can be detected in the resonant frequency and amplitude changes of the reflection coefficient S_{11}. However, it has been generally known that a Love wave device has very low vertical radiation energy loss in contact with liquid. Since the particle displacement in the SH mode is parallel to the device surface and normal to the direction of propagation, there is no acoustic coupling loss. To find how much acoustic energy is lost in liquid, we dipped the fabricated device into PBS solution and then compared the S_{11} reflection peaks before and after liquid infusion. As shown in figure 10, nearly negligible differences between two results were observed, confirming that our Love wave device is very stable in liquid contact. Next, the device was placed in liquid solution for long period to test for swelling of the PMMA waveguide layer due to the absorption of water, which can cause a deterioration of the device. However, in tests, no significant changes were observed in the resonance frequency and amplitude of S_{11}.

5.5. Protein A immobilization measurement

Protein A molecules were immobilized onto the gold surface to create the receptor layer. To evaluate the surface topography of the protein A film, atomic force microscope (AFM) and scanning electron microscope (SEM) measurements were performed before and after the immobilization. As shown in figure 11(a), the AFM peaks have the same height and are well distributed on the sample surface, indicating a uniform coverage of protein A. In the SEM image, dense protein A molecules were also observed on the gold surface (figure 11(b)). Also, the mass loading effect from the protein A immobilization onto the gold surface induces an acoustic wave velocity change, and results in the time deviation of the second and third reflection peaks, as shown in figure 11(c). No clear time shift was observed in the first reflection peaks, which were used as the reference. Much washing and rinsing of the sample in PBS was performed to check if the protein A molecules were strongly bound onto the gold surface. The reflection coefficient S_{11} was wirelessly measured using the network analyzer in air at room temperature. The amplitude and time positions of the S_{11} peaks were almost the same as the results obtained before thoroughly washing and rinsing, suggesting that protein A is strongly immobilized on the gold surface.

5.6. Sensitivity evaluation

The fabricated devices with various PMMA guiding layer thicknesses were dipped into various IgG solutions in the concentration range 1–65 nM. The reflection peak S_{11} was monitored by the network analyzer at conditions of 25 °C and ∼20 cm request distance. The binding of the IgG to the protein

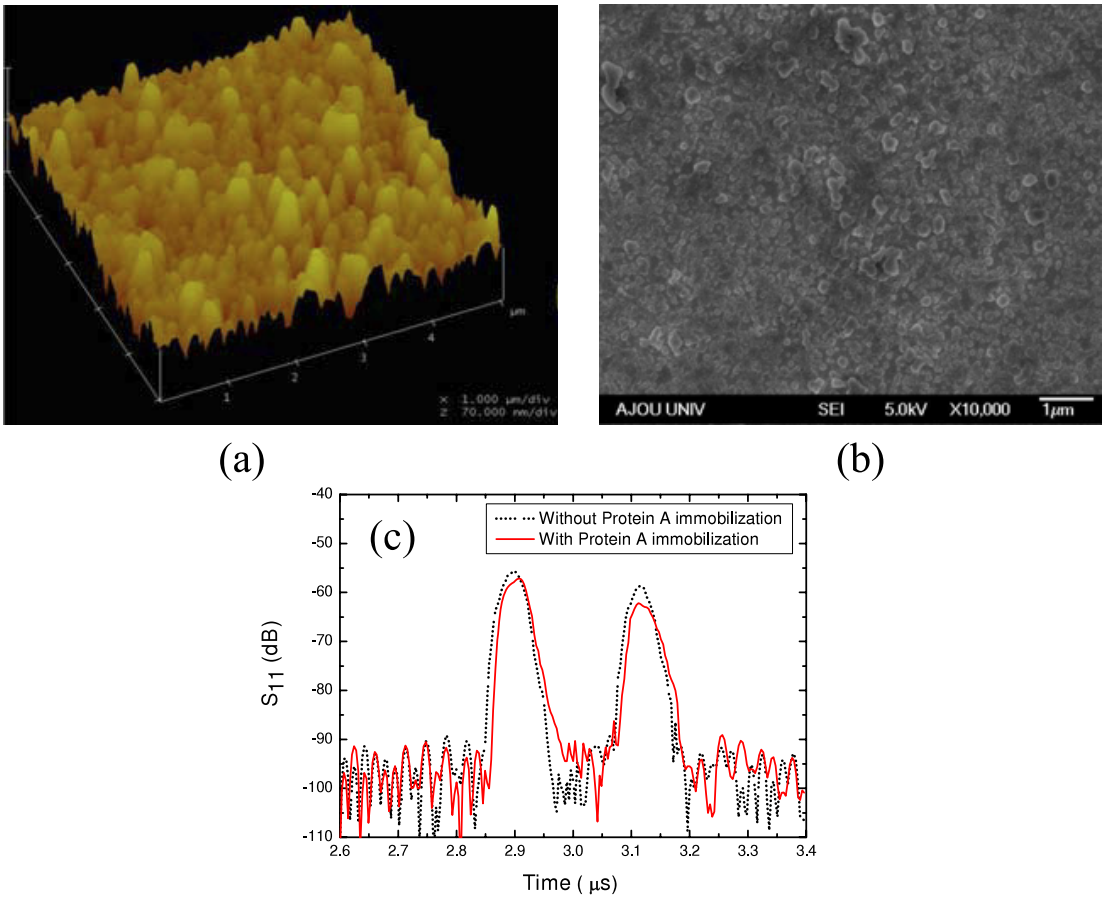

Figure 11. (a) AFM image of protein A surface, (b) SEM image of immobilized protein A molecules on the gold surface, and (c) the measured S_{11} in cases with and without protein A immobilization.

A modified gold surface induced the time deviations of the reflection peaks. The time deviation, $\Delta\tau$, was changed to the phase angle shift, $\Delta\Phi$, using equation (5), because the phase shift provides much higher resolution than the time shift of the reflection peak. The phase shift due to the IgG binding was evaluated through the difference of method (DOM) of equation (6). Figure 12 shows the phase shifts of the fabricated biosensor in terms of the time depending on different PMMA thicknesses (0.9, 1.5, 2 μm) for a constant 40 nM IgG solution. Here, the phase angle shifts were recorded every 1 min, so one point on the graph corresponds to a 1 min interval. It is obvious that the phase shift increases with waveguide thickness in the range 0.9–1.5 μm, whereas, for thicker guiding layer thickness ($\sim$2 μm), the phase shift decreases. The sensor with 1.5 μm PMMA guiding layer shows the highest phase response. From these experimental results, we suggest that the optimal PMMA waveguide thickness is $\sim$1.5 μm, which agrees well with the theoretical results.

Also, the reproducibility of the fabricated sensor with 1.5 μm thick PMMA guiding layer was tested in 40 nM IgG solution, where the gold surface was modified by a protein A concentration of 50 mg ml^{-1}. As shown in figure 13(a), the average phase shifts show $\sim$5% deviation values from five experimental tests, suggesting that the fabricated sensor has good reproducibility. Using a sensor with a $\sim$1.5 μm PMMA thickness, the phase angle shift of the reflection peaks

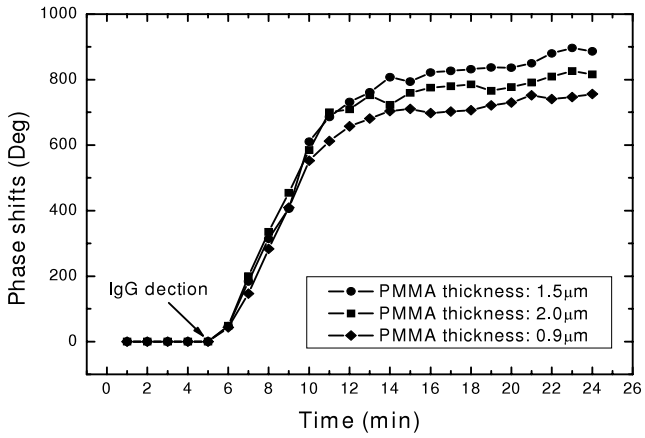

Figure 12. Comparison of sensor phase response depending on the PMMA waveguide layer thickness at the IgG concentration of 40 nM.

depending on different IgG concentrations (0–65 nM) was investigated (figure 13(b)). For these IgG concentration ranges, the phase shifts showed nearly linear behavior with increasing IgG concentrations. The evaluated sensitivity of the sensor was $\sim$17.5°/nM. From these promising results, we believe that the Love wave devices are promising for improving the sensitivity of the biosensor.

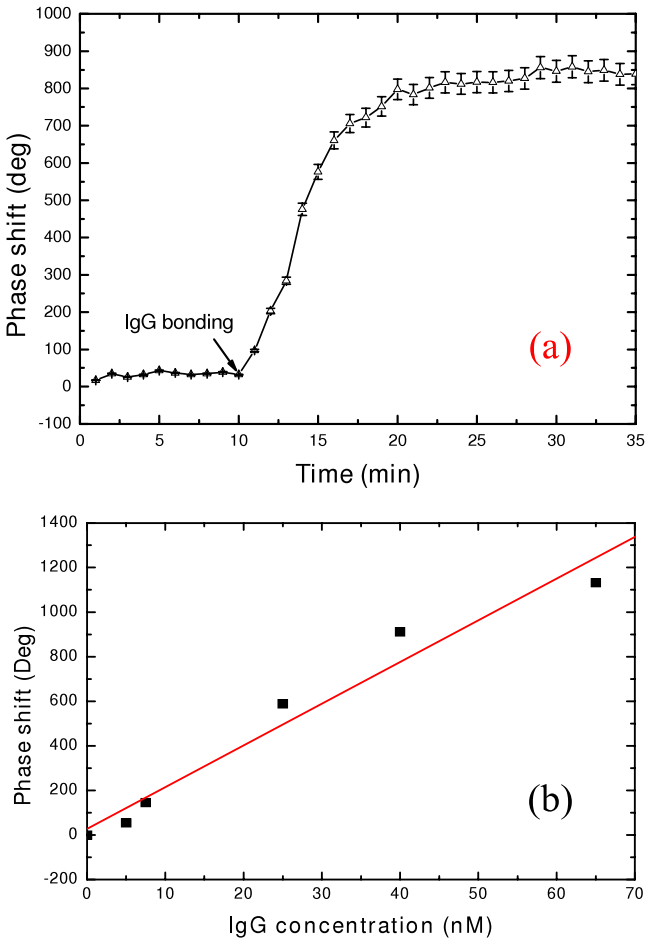

Figure 13. (a) Reproducibility results of the fabricated sensor in a constant 40 nM IgG solution, (b) phase response of the fabricated sensors in the IgG concentration range 0–65 nM.

6. Conclusion

A novel wireless biosensor incorporating a waveguide mode reflective delay line on 41° YX $LiNbO_3$ was successfully demonstrated. PMMA was used as the waveguide layer due to its lower bulk velocity and lower density. Using the network analyzer as the reader unit, the fabricated sensor was wirelessly characterized. Phase shifts were clearly observed due to the binding of different IgG concentrations to the protein A modified gold surface. Good linearity, reproducibility, and high sensitivity were observed. The evaluated sensitivity was approximately 17.5°/nM.

References

[1] Jakoby B and Vellekoop M J 1997 Properties of Love waves: applications in sensors *Smart Mater. Struct.* **6** 668–79

[2] Kovacs G, Vellekoop M J and Hauels R 1992 Love wave sensor for (bio) chemical sensing in liquids *IEEE Ultrason. Symp.* pp 281–5

[3] Kovacs G, Vellekoop M J and Hauels R 1994 Love waves for (bio) chemical sensing in liquids *Sensors Actuators* A **43** 38–43

[4] Jakoby B and Vellekoop M J 1998 Analysis and optimization of Love wave liquid sensors *IEEE Trans. Ultrason. Ferroelectr. Freq. Control* **45** 1293–302

[5] Herrmann F, Weihnacht M and Buttgenbach S 1999 Properties of sensors based on shear-horizontal surface acoustic waves in different layered quartz–SiO_2 structures *Ultrasonic* **37** 335–41

[6] Herrmann F, Weihnacht M and Buttgenbach S 2001 Properties of sensors based on shear-horizontal surface acoustic waves in $LiTaO_3/SiO_2$ and quartz/SiO_2 structures *IEEE Trans. Ultrason. Ferroelectr. Freq. Control* **48** 268–73

[7] Harding G, Du J and Dencher P 1997 Love wave acoustic immunosensor operating in liquid *Sensors Actuators* A **61** 279–86

[8] Tamarin O, Comeau S and Dejous C 2003 Real time device for biosensing: design of a bacteriophage model using Love acoustic waves *Biosens. Bioelectron.* **18** 755–63

[9] Gizeli E 1997 Design considerations for the acoustic waveguide biosensor *Smart Mater. Struct.* **6** 700–6

[10] Bender F, Cernosek R W and Josse F 2000 Love-wave biosensors using cross-linked polymer waveguides on $LiTaO_3$ substrate *Electron. Lett.* **36** 1672–3

[11] Rasmusson A and Gizeli E 2001 Comparison of PMMA and Novolak waveguide coatings for an acoustic biosensor *J. Appl. Phys.* **90** 5911–4

[12] McHale G, Newton M I and Martin F 2001 Resonant conditions for Love wave guiding layer thickness *Appl. Phys. Lett.* **79** 3542–3

[13] Gizeli E, Bender F and Rasmusson A 2003 Sensitivity of the acoustic waveguide biosensor to protein binding as function of the waveguide properties *Biosens. Bioelectron.* **18** 1399–406

[14] Branch D W and Brozik S M 2004 Low-level detection of a bacillus anthracis stimulant using Love-wave biosensors on 36° YX $LiTaO_3$ *Biosens. Bioelectron.* **19** 849–59

[15] Harding G L and Du J 1997 Design and properties of quartz-based Love wave acoustic sensors incorporating silicon dioxide and PMMA guiding layers *Smart Mater. Struct.* **6** 716–20

[16] Du J and Harding G L 1998 A multilayer structure for Love-mode acoustic sensors *Sensors Actuators* A **65** 152–9

[17] Martin S J and Frye G C 1994 Dynamics and response of polymer-coated surface acoustic wave devices: effect of viscoelastic properties and film resonance *Anal. Chem.* **66** 2201–19

[18] Hashimoto K 2000 *Surface Acoustic Wave Devices in Telecommunications—Modeling and Simulation* (New York: Springer)

[19] Gizeli E, Goddard N J and Lowe C R 1992 A Love-plate biosensor utilizing a polymer layer *Sensors Actuators* B **6** 131–7

[20] Wang W, Lee K, Woo I, Park I and Yang S 2007 Optimal design on SAW sensor for wireless pressure measurement based on reflective delay line *Sensors Actuators* A **139** 2–6

[21] Royer D and Dieulesaint E 2000 *Elastic Waves in Solids* (Heidelberg: Springer)

[22] Zimmermann C, Rebiere D and Dejous C 2002 Love-waves to improve chemical sensors sensitivity: theoretical and experimental comparison of acoustic modes *IEEE Int. Frequency Control Symp.* pp 281–8

[23] Kielczynski P 1997 Attenuation of Love waves in low-loss media *J. Appl. Phys.* **82** 5932–7

[24] Jungwirth M, Scherr H and Weigel R 2002 Micromechanical precision pressure sensor incorporating SAW delay lines *Acta. Mech.* **158** 227–52

[25] Auld B 1973 *Acoustic Fields and Waves in Solids* vol 1 (New York: Wiley)

[26] Reindl L and Shrena I 2004 Wireless measurement of temperature using surface acoustic waves sensors *IEEE Trans. Ultrason. Ferroelectr. Freq. Control* **51** 1457–63